The Design of Broadband Circularly Polarized Multi-beam Antenna with Linearly Polarized Feeding Source and Transmitarray Unit

Zexu GUO, Yulong ZHOU, Huanhuan YANG, Sijia LI, Tong LI, Xiangyu CAO

Information and Navigation College of Air Force Engineering University, Xi'an, Shaanxi, 710077, China

418604809@qq.com

Submitted August 21, 2023 / Accepted December 14, 2023 / Online first December 21, 2023

Abstract. *Among the existing circularly polarized multi-beam transmitarray antennas, circularly or linearly-to-circularly polarized transmitarray units are always required. Naturally, designing circularly polarized units is more challenging than linear polarization. To simplify design and increase operation bandwidth, a novel method using linearly polarized transmitarray units and feeding sources is proposed for designing the circularly polarized multi-beam antenna. Broadband circular polarization is realized by utilizing sequential rotation technology and 1-bit phase compensation of linearly polarized transmitarray units. Meanwhile, beam scanning is achieved by using linearly polarized feeding sources offset. To validate the design, two multi-beam antenna samples are demonstrated. Simulated and measured results show that the designed multi-beam transmitarray antennas can realize beam scanning to 0°, ±10°, and ±20° in E-plane and H-plane. Moreover, two antennas maintain –10-dB impedance bandwidth and 3-dB axial ratio (AR) bandwidth at 8.5–10.4 GHz and 8.5–10.5 GHz, respectively. The proposed circularly polarized multi-beam transmitarray antennas have the advantages of broadband operation, simple design, and low cost.*

Keywords

Circular polarization, multi-beam antenna, spatial feed, transmitarray antenna

1. Introduction

With the increasing congestion of low-frequency spectrum resources and the explosive growth of communication data, the utilization of high-frequency spectrum becomes more urgent. High-gain antennas are widely used to overcome the severe attenuation of electromagnetic wave propagation at high-frequency bands. However, the high-gain antenna is achieved at the expense of beam width, resulting in reduced beam coverage. A multi-beam antenna can generate multiple radiation beams to expand the space coverage in a shared aperture [1–5]. In recent years, elaborately engineered transmitarrays have been manifested to enlarge the beam coverage and reduce gain loss [6–9]. Besides, the circularly polarized multi-beam antenna is widely used in satellite communication, radar systems, and MIMO communication [10–14].

The circularly polarized multi-beam antenna can be divided into active and passive designs according to whether it can be controlled electrically. The active multi-beam antenna needs many expensive phase shifters [15, 16, 17]. The passive multi-beam antenna can be divided into spatial feed [18] and matrix network feed [19–22] according to different feeding modes. The broadband design of complex matrix network feed is challenging. The space-fed multi-beam antenna is based on the optical principle, which can easily realize beam scanning using feeding sources offset. The space-fed multi-beam antennas are divided into reflection and transmission modes according to the relative position of feeding sources and radiation beams. In particular, the multi-beam transmitarray antenna is free of feeding source occlusion.

Generally, there are two methods to design circularly polarized multi-beam transmitarray antenna:

1) Circularly polarized feeding sources and circularly polarized transmitarray units are adopted [18], [23–25].

2) Linearly polarized feeding sources are adopted, and the transmitarray units can convert linear to circular polarization [26–29].

Undoubtedly, designing circularly polarized feeding sources is more complicated than linear polarization. More importantly, the broadband design of circularly or linearly-to-circularly polarized transmitarray units is challenging because a high transmission coefficient must be maintained in the frequency band of axial ratio (AR) less than 3 dB.

This paper proposes a novel method using linearly polarized feeding sources and transmitarray units to design circularly polarized multi-beam antenna. Broadband circular polarization is realized by utilizing sequential rotation technology and 1-bit phase compensation of linearly polar-

DOI: 10.13164/re.2024.0136

ized transmitarray units. The proposed method reduces the design difficulty and increases circularly polarized operating bandwidth, simultaneously. Two transmitarray antenna samples are measured to verify the proposed methods. Simulated and measured results show that the designed multi-beam transmitarray antennas possess distinguished port isolation performance and broadband circularly polarized radiation characteristics.

2. Simulation of Transmitarray Unit

A schematic diagram of the proposed circularly polarized multi-beam transmitarray antenna is shown in Fig. 1. The antenna comprises a transmitarray and feeding source. To simplify the design, linearly polarized feeding sources are adopted, and multiple beams are obtained using feeding sources offset. To realize high-gain circularly polarized radiation, the transmitarray needs to realize two functions:

1) The phase difference introduced by spatial feed is compensated, and the spherical phase front is converted into the planar phase front.

2) The linearly polarized wave from feeding sources is converted into the circularly polarized wave.

In the proposed method, the two functions above are simultaneously realized by arranging the linearly polarized transmitarray unit.

The transmitarray unit using a receiver-transmitter structure is shown in Fig. 2(a). The blue part is the dielectric layer ($\varepsilon_r = 2.55$, $\tan\delta = 0.002$, $h = 1.524$ mm), the yellow part is the metal layer, and the green part is the bonded layer ($\varepsilon_r = 3.58$, $\tan\delta = 0.004$, $h_1 = 0.1$ mm). The E-shape metal patches work as receiving and transmitting antennas. A metal ground is placed to isolate two E-shape metal patches. Parameters of the unit are $p = 10$ mm, $w = 8.1$ mm, $l = 8.1$ mm, $dw = 1.8$ mm, $dl = 2$ mm, $w_1 = 1.2$ mm, $w_2 = 1.2$ mm, $r_1 = 1$ mm, $r_2 = 1.6$ mm, and $r_3 = 1.4$ mm.

The transmitarray unit is simulated in HFSS 19.0 with infinite periodic boundary conditions. Two ports are set, and electromagnetic waves are vertically incident to excite the transmitarray unit. T_{yx} and R_{yx} represent cross-polarization transmission and reflection components, respectively. Accordingly, T_{xx} and R_{xx} represent co-polarization transmission and reflection components, respectively. The co-polarization transmission ratio (TR) can be expressed as

$$TR = \frac{T_{xx}^2}{T_{xx}^2 + T_{yx}^2 + R_{xx}^2 + R_{yx}^2}. \quad (1)$$

The unit's simulated propagation coefficients and TR are shown in Fig. 2(b). TR is higher than 97% at 8.7–10.3 GHz. The middle metal ground can isolate the upper and bottom E-shape metal patches. Therefore, when changing the polarization direction of the upper E-shaped patch to y-polarization, the TR of the unit will hardly change regardless of the polarization of the upper E-shape metal patches, as shown in Fig. 2(b). Besides, when the bottom E-shape metallic patch is rotated 0° or 180°, a 1-bit transmission phase resolution can be realized, as demonstrated in Fig. 2(c).

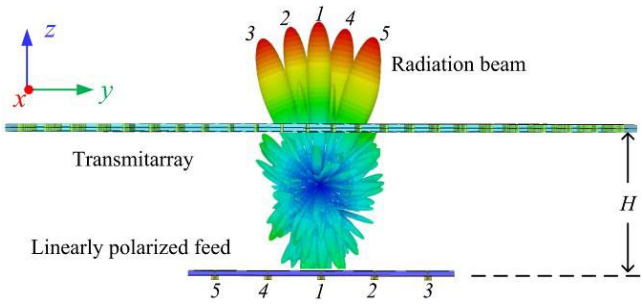

Fig. 1. Schematic diagram of the proposed multi-beam transmitarray antenna.

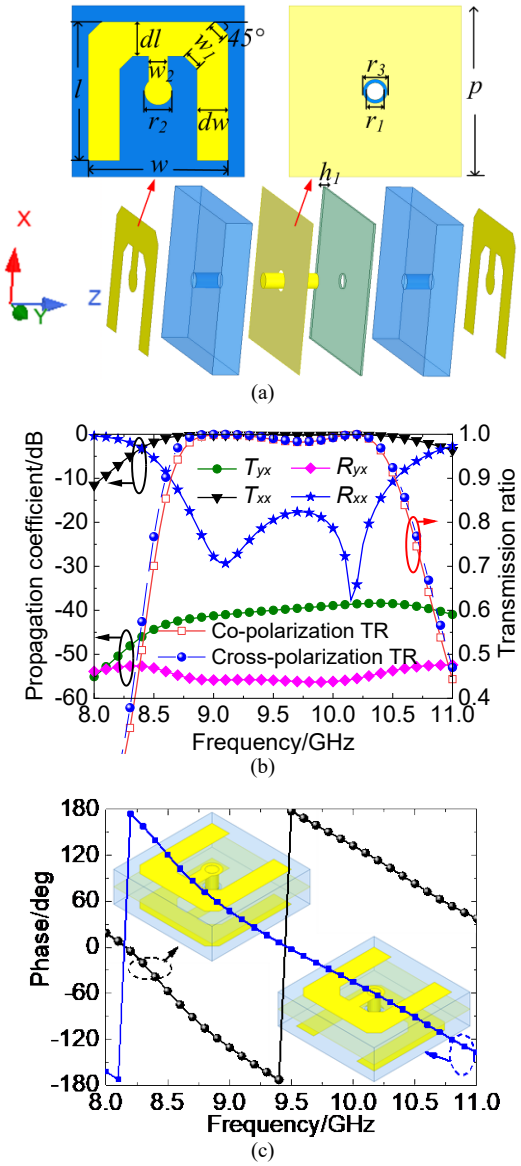

Fig. 2. (a) Schematic diagram of the transmitarray unit. (b) Propagation coefficients and TR of the transmitarray unit. (c) 1-bit phase resolution of the transmitarray unit.

In Fig. 2(b), two resonance frequencies appear at 9.1 and 10.2 GHz. Different from impedance cascade analysis [30], the structure is analyzed as two linearly polarized microstrip antennas connected back-to-back. One side of the microstrip antenna receives the electromagnetic wave from the feeding source. Then, the energy is transmitted by a metallic via in the middle of the unit. Finally, another side of the microstrip antenna radiates energy. The current analysis at two resonant frequencies is performed, as depicted in Fig. 3. At low frequency (9.1 GHz), the current flows around the slot to the metal arms with a long current path. At high frequency (10.2 GHz), the current flows parallel on metal arms. The unit presents a wide operating band because of combining two resonance frequencies.

The unit's parameters were analyzed to prove the current analysis, as shown in Fig. 4. Theoretically, the adjustment of the metal arm width (*dw*) will affect the current path at low frequency. The high-frequency current flows along the long side of the metal arm. Therefore, there is negligible effect at high frequency, as shown in Fig. 4(a). The parameter scanning of metal arm length (*dl*) will simultaneously change the current path of two resonant frequencies. Accordingly, Figure 4(b) shows that both resonant frequencies are changed.

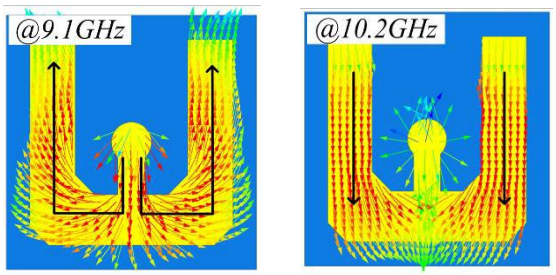

Fig. 3. The current analysis at two resonant frequencies.

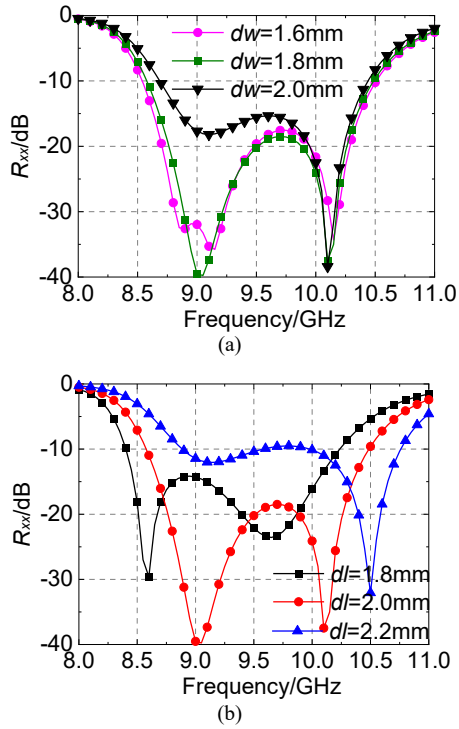

Fig. 4. The parameters analysis of the unit. (a) Width of metal arm (*dw*). (b) Length of metal arm (*dl*).

3. Design of Transmitarray

According to polarization theory, circular polarization can be regarded as an elliptical polarization with a small AR, and linear polarization can be regarded as an elliptical polarization with a large AR. For simplicity and without loss of generality, suppose the unit radiates a left-handed elliptically polarized wave ($\mathbf{E}_{\text{cell}}$)

$$\mathbf{E}_{\text{cell}} = a\cdot\mathbf{x} + jb\cdot\mathbf{y} \tag{2}$$

where $\mathbf{x}$ and $\mathbf{y}$ represent normalized vectors along the *x*-axis and *y*-axis, respectively, *a* and *b* represent the amplitudes in two vertical directions. As shown in Fig. 5(a), when four units are uniformly arranged with the same feeding phase, the total electric field is $\mathbf{E}'$

$$\mathbf{E}' = 4\times\left(a\cdot\mathbf{x} + jb\cdot\mathbf{y}\right). \tag{3}$$

Based on (3), the polarization characteristics of the sub-array are completely dependent on the unit. The transmitarray unit must radiate circularly polarized wave to realize sub-array's circular polarization. However, it is difficult to design a circularly polarized unit with high TR and low AR in a broadband range. Therefore, the sequential rotation technology [31], [32] is adopted to realize circularly polarized radiation, as shown in Fig. 5(b). The four units are rotated sequentially with a 90° phase gradient along left-hand rotation. At the same time, the feeding phases also differ by 90° phase gradient along left-hand rotation. Hence, $\mathbf{E}_1$, $\mathbf{E}_2$, $\mathbf{E}_3$ and $\mathbf{E}_4$ can be written as

$$\begin{aligned}
\mathbf{E}_1 &= \left(a\cdot\mathbf{x} + jb\cdot\mathbf{y}\right)\cdot\mathrm{e}^{\mathrm{j}0} = a\cdot\mathbf{x} + jb\cdot\mathbf{y},\\
\mathbf{E}_2 &= \left(-jb\cdot\mathbf{x} + a\cdot\mathbf{y}\right)\cdot\mathrm{e}^{\mathrm{j}\cdot 90^\circ} = b\cdot\mathbf{x} + ja\cdot\mathbf{y},\\
\mathbf{E}_3 &= \left(-a\cdot\mathbf{x} - jb\cdot\mathbf{y}\right)\cdot\mathrm{e}^{\mathrm{j}\cdot 180^\circ} = a\cdot\mathbf{x} + jb\cdot\mathbf{y},\\
\mathbf{E}_4 &= \left(jb\cdot\mathbf{x} - a\cdot\mathbf{y}\right)\cdot\mathrm{e}^{\mathrm{j}\cdot 270^\circ} = b\cdot\mathbf{x} + ja\cdot\mathbf{y}.
\end{aligned} \tag{4}$$

At $\theta = 0°$, the total electric field is $\mathbf{E}$

$$\mathbf{E} = \mathbf{E}_1 + \mathbf{E}_2 + \mathbf{E}_3 + \mathbf{E}_4 = \left(2a + 2b\right)\left(\mathbf{x} + \mathrm{j}\mathbf{y}\right). \tag{5}$$

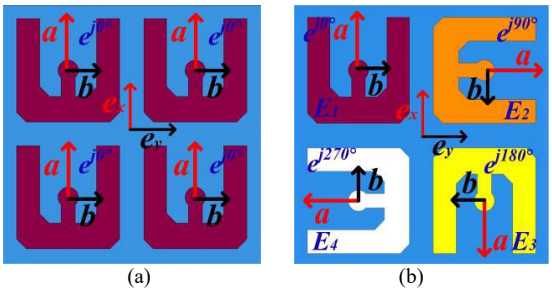

Fig. 5. The sub-array arrangement of transmitarray unit. (a) Uniform configuration. (b) Sequential rotation configuration.

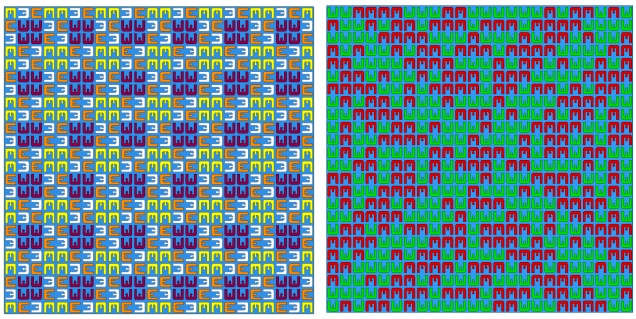

(a) (b)

Fig. 6. The arrangement of E-shape metallic patches. (a) Upper layer of the transmitarray. (b) Bottom layer of the transmitarray.

According to (5), the sub-array possesses an inherent circular polarization characteristic, which is independent of the unit polarization. Theoretically, even if a linearly polarized unit is adopted, the sub-array can still realize the circularly polarized radiation.

Based on the above sub-array analysis, a transmitarray consisting of 24 × 24 units (240 mm × 240 mm) is designed. A second-order sequence rotation arrangement [33] is used for the upper E-shape metal patches to realize circular polarization, as shown in Fig. 6(a). According to the operation principle of sequence rotation arrangement, the unit (m, n) should satisfy the corresponding sequence rotation feeding phase ($\varphi_{C,mn}$). Besides, the space-fed phase difference of unit (m, n) should be considered, which can be written as

$$\varphi_{S,mn} = k_0(\sqrt{x^2 + y^2 + F^2} - F). \tag{6}$$

The focal diameter ratio (F/D) is selected as 0.5. Hence, the focal length (F) is 120 mm. The total compensation of space-fed phase ($\varphi_{S,mn}$) and sequence rotation feeding phase ($\varphi_{C,mn}$) can be expressed as

$$\varphi_{T,mn} = -\varphi_{S,mn} + \varphi_{C,mn} + \mathbf{u}_0 \cdot \mathbf{r}_{mn}. \tag{7}$$

When achieving beam focus at the broadside, the last term of (7) is null. The total compensation phase ($\varphi_{T,mn}$) can be implemented by rotating bottom E-shape metallic patches with 0° or 180°. According to (7), the 1-bit coding arrangement of bottom E-shape metallic patches can be calculated in MATLAB, as shown in Fig. 6(b).

4. Multi-beam Transmitarray Antenna

It is worth noting that the polarization of the bottom E-shape metal patches is the same. Therefore, linearly polarized antennas can be used as feeding sources. A microstrip patch array with four U-shape slots is adopted, as shown in Fig. 7(a). The detailed parameters are $p_2 = 28$ mm, $m_1 = 1.9$ mm, $m_2 = 3.8$ mm, $m_3 = 10.4$ mm, $n_1 = 8$ mm, and $n_2 = 6.1$ mm. The simulated and measured S11 possess two resonance frequencies, and the measured operating frequency is 8.5–10.5 GHz, as shown in Fig. 7(b). At 9.5 GHz,

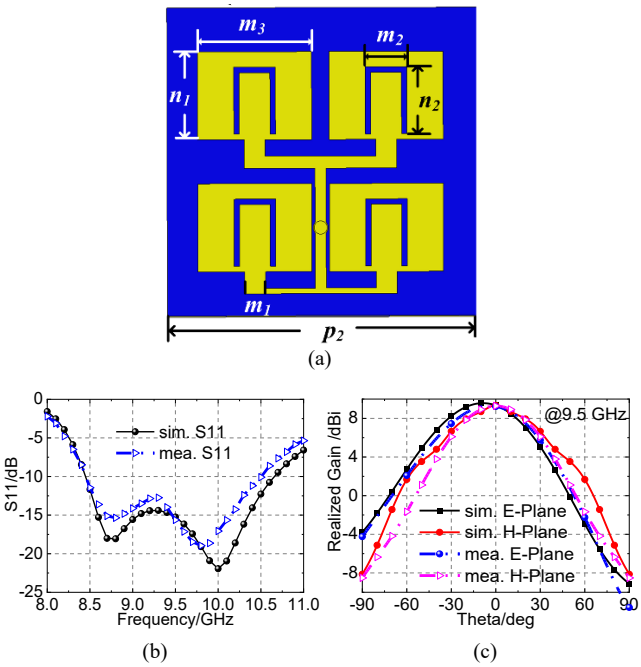

(a) (b) (c)

Fig. 7. The designed feeding source: (a) Configuration of linearly polarized antenna. (b) The simulated and measured reflection coefficient. (c) The simulated and measured radiation pattern in the E-plane and H-plane.

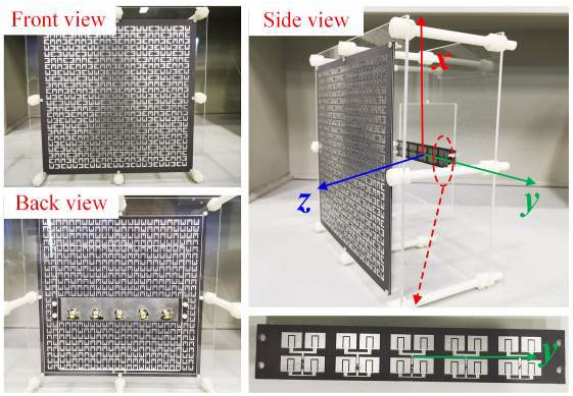

(a)

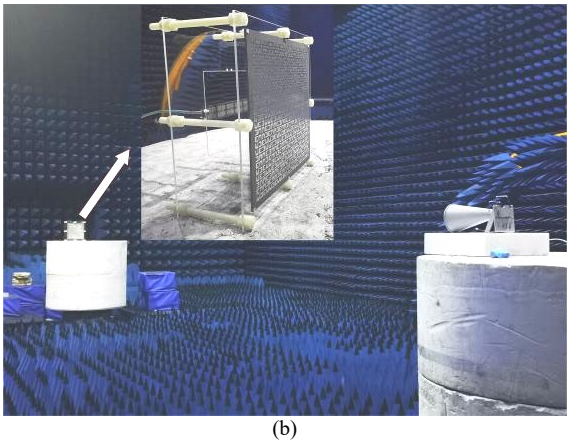

(b)

Fig. 8. (a) The experimental antenna prototype. (b) Practical measurements in microwave anechoic chamber.

the simulated and measured radiation patterns fit well in both the E-plane and H-plane, as plotted in Fig. 7(c).

The prototype of a five-beam transmitarray antenna is fabricated, as shown in Fig. 8(a). It comprises a transmitarray and five linearly polarized feeding sources along the *y*-axis. The distance between the feeding sources and the transmitarray is controlled by several nylon screws. Practical measurement is carried out in an anechoic chamber, as shown in Fig. 8(b).

The measured reflection and port isolation coefficients are shown in Fig. 9. At 8.5–10.4 GHz, the transmitarray antenna has two resonant frequencies. Meanwhile, high isolation among five ports is realized in the working frequency band, and mutual couplings between any two ports are lower than –18 dB.

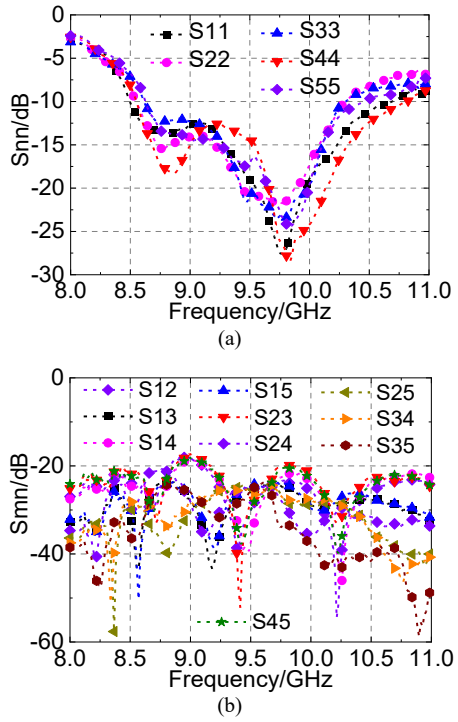

Fig. 9. Measured results of five-beam transmitarray antenna. (a) Reflection coefficient. (b) Port isolation coefficient.

The feeding sources are located along the *y*-axis. Switching the feeding port along the *y*-axis, the space-fed phase difference of unit (*m*, *n*) can be expressed as [23]

$$\varphi_{S,mn} = k_0\sqrt{x^2+(y-d)^2+F^2}-\sqrt{F^2+d^2} \qquad (8)$$

where *d* indicates the moving distance of the feeding port. In this case, the total transmission phase of unit (*m*, *n*) is written as

$$\varphi_{OUT,mn} = \varphi_{S,mn}+\varphi_{T,mn} = k_0\left[\sqrt{x^2+(y-d)^2+F^2}-\sqrt{F^2+a^2}\right]- k_0\left[\sqrt{x^2+y^2+F^2}-F\right]+\varphi_{C,mn}. \qquad (9)$$

To simplify the analysis, equation (9) can be expressed as ($x = 0$):

$$\varphi_{OUT,mny} = k_0\sqrt{(y-d)^2+F^2}-k_0\sqrt{y^2+F^2}+c \qquad (10)$$

where *c* is an angle constant that does not depend on *y*. After equation (10) is further simplified, it can be written as

$$\frac{\varphi_{OUT,mny}-c}{k_0} = \sqrt{(y-d)^2+F^2}-\sqrt{y^2+F^2}. \qquad (11)$$

With *y*/*F* as the variable, two curves ($d = -0.2F$ and $d = 0.4F$) are drawn according to (11), as shown in Fig. 10 (dashed line). After the feeding ports are switched, the total transmission phase approximately presents a linear change. The beam scanning angle in the H-plane can be expressed as

$$\theta_d = \arcsin\left(\frac{\lambda_0}{2\pi}\cdot\frac{\partial\varphi_{OUT,mny}}{\partial y}\right) = \arcsin\left(\frac{1}{k_0}\cdot\frac{\partial\varphi_{OUT,mny}}{\partial y}\right). \qquad (12)$$

According to (12), the slope of dashed lines (in Fig. 10) represents the scanning angle, which varies with the change of *d*. Hence, beam scanning can be realized by switching the feeding port. Moreover, *d* can be positive or negative, indicating positive or negative scanning angle. The solid line (in Fig. 10) represents the maximum slope of the dashed line, which corresponds to an ideal maximum scanning angle. Apparently, there is an inconsistency between the dashed lines and solid lines, which suggest an inherent phase distortion of the transmitarray. Moreover, when units are close to the edge of the transmitarray, the phase distortion is larger. On the other hand, when the absolute value of *d* increases, the phase distortion becomes more obvious. All in all, because of the existing phase distortion, the actual scanning angle is less than the ideal maximum.

The simulated and measured radiation pattern of five beams at 9.3 GHz and 10.2 GHz are shown in Fig. 11. The left-hand circularly polarized (LHCP) beams point to –20° (beam 3, B3), –10° (beam 2, B2), 0° (beam 1, B1), 10° (beam 4, B4), and 20° (beam 5, B5), respectively. According to (12), the calculated ideal scanning angle of beam 4 is 13.4°, while the actual scanning angle is less than the ideal maximum, which is consistent with the theoretical analysis above.

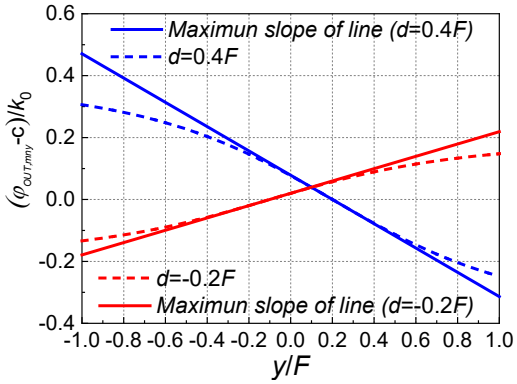

Fig. 10. The total transmission phase distribution of $d = -0.2F$ and $d = 0.4F$.

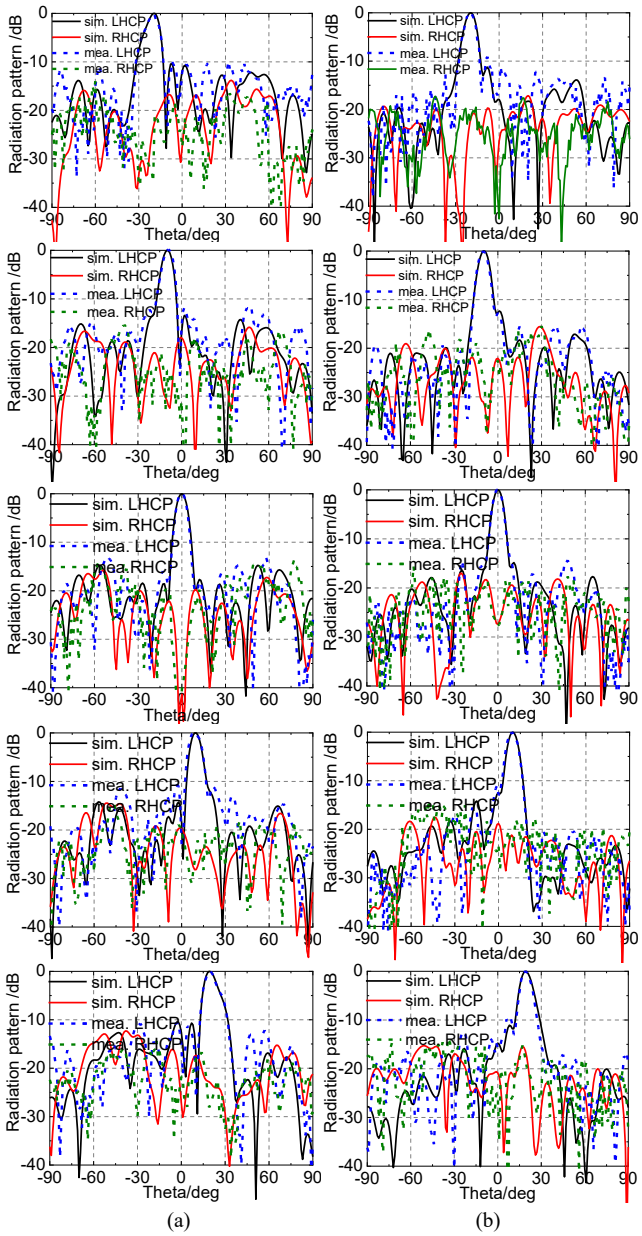

Fig. 11. Simulated and measured radiation pattern in *yoz*-plane: (a) at 9.3 GHz and (b) 10.2 GHz.

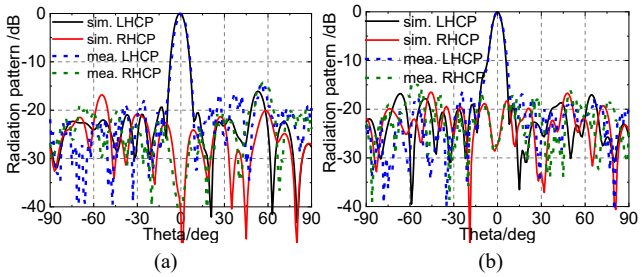

Fig. 12. The broadside radiation beam in *xoz*-plane: (a) at 9.3 GHz and (b) 10.2 GHz.

The amplitude of the LHCP wave is much higher than the right-hand circularly polarized (RHCP) wave in the prescribed beam direction. The five-beam transmitarray antenna presents high-gain circularly polarized radiation performance. Meanwhile, the broadside beams are measured in the *xoz*-plane, as shown in Fig. 12. Pencil beams with excellent left-hand circularly polarized performance are demonstrated at 9.3 GHz and 10.2 GHz. The proposed antenna is characterized by high directivity in both E-plane and H-plane. Due to the impact of the test environment, fabrication, and assembly errors, the variation of simulated and measured results is within a reasonable range.

The realized gain of the broadside beam is simulated and measured from 8 GHz to 10 GHz to verify the broadband performance. In Fig. 13(a), the peak realized gain of beam 1 (B1) is 22.5 dBi at 9.7 GHz. For an aperture antenna with the size of 240 mm × 240 mm, the ideal directivity is $D = 4\pi A/\lambda_0^2$, where A is the aperture area, and λ_0 is the corresponding wavelength of 9.7 GHz. The calculated D is 28.8 dB. Hence, the aperture efficiency ($\eta_a = G/D$) of the transmitarray antenna is 23.5% at 9.7 GHz. Besides, the realized gain shows a relatively smooth trend, and the high gain is maintained in a wide frequency band. The 2-dB gain bandwidth is 9.2–10.2 GHz.

The AR of beam 1 (B1) changing with frequency is shown in Fig. 13(b). The simulated and measured results show that the transmitarray antenna can achieve circularly polarized radiation with AR lower than 3 dB at 8.5–10.5 GHz. In the wide operating band, the measured realized gain and AR are in good agreement with the simulation. The error between measurement and simulation does not affect the correctness and effectiveness of the proposed design. Meanwhile, the feeding sources can also be arranged along the *x*-axis, and a five-beam transmitarray antenna with the ability of E-plane scanning can be realized, as shown in Fig. 14.

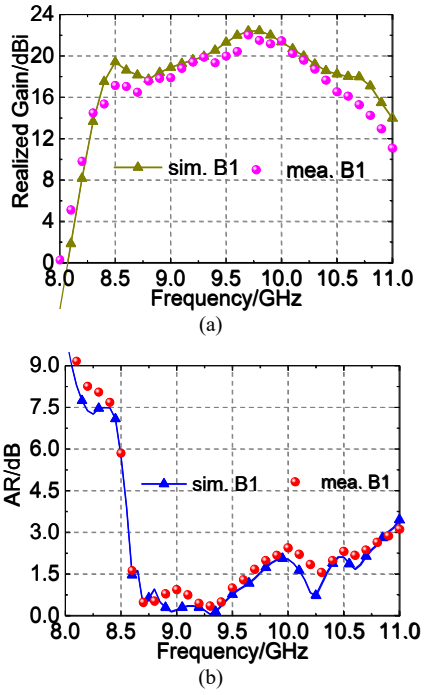

Fig. 13. Broadband performance of the transmitarray antenna in the broadside: (a) Realized gain. (b) *AR*.

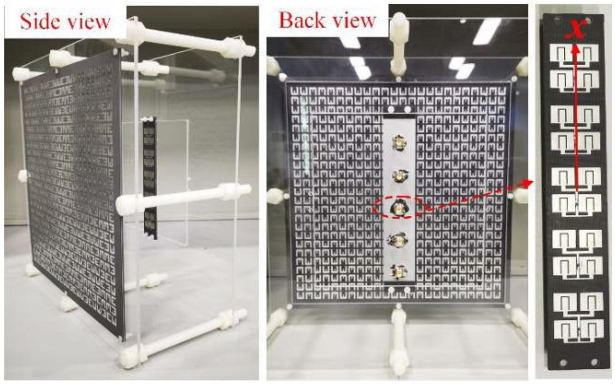

Fig. 14. Five-beam transmitarray antenna with the ability of E-plane beam scanning.

Figure 15(a) shows the simulated and measured gain pattern at 9.7 GHz. The five beams point to –20°, –10°, 0°, 10°, and 20° in the *xoz*-plane, and the scanning gain decreases within 3.6 dB. The main reason for the decrease in scanning gain is that the 1-bit compensation phase arrangement of the transmitarray aims to achieve a maximum gain in the broadside. When the feeding source is offset, the inherent phase distortion is introduced, as mentioned in Fig. 10. This phenomenon can be alleviated using a multi-focus design of the transmitarray. However, the multi-focus design will lead to a gain decrease in the broadside. Therefore, making a tradeoff according to the design requirements is necessary. Figure 15(b) shows the AR of five beams, which suggests that five beams possess good circularly polarized characteristics in the prescribed direction.

To highlight the novelty and advantages of this work, a comparison is concluded in Tab. 1. Among the existing circularly polarized multi-beam transmitarray antenna, the circularly or linearly-to-circularly polarized transmitarray unit is always required. Different from the other circularly polarized multi-beam transmitarray antennas, the proposed transmitarray antennas are based on the linearly polarized feeding source and transmitarray unit. The proposed method can effectively reduce the design difficulty. Furthermore, among most existing prototypes, SIW (Substrate Integrated Waveguide) antennas and horn antennas are used as feeding sources to alleviate port coupling and pursue broadband operation. Compared with the microstrip antenna, the SIW antennas possess a more complex structure, and the horn antennas inevitably increase the overall profile of the designed antenna. This work uses only low-profile microstrip antennas as feeding sources to achieve broadband circularly polarized operation with satisfactory port isolation.

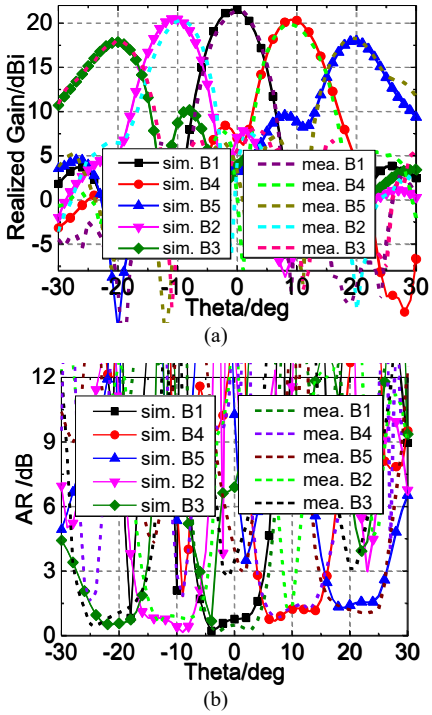

Fig. 15. The radiation performance of five-beam transmitarray antenna in the *xoz*-plane. (a) Radiation pattern; (b) *AR*.

5. Conclusion

In summary, this work demonstrates a novel method for designing circularly polarized multi-beam transmitarray antennas, and two multi-beam transmitarray antenna prototypes are designed, fabricated, and measured. Different from the other circularly polarized multi-beam transmitarray antennas, the proposed antennas are based on the linearly polarized feeding source and transmitarray unit. This new method increases the operating bandwidth and reduces the design difficulty, simultaneously. To highlight the novelty and advantages of this work, a comparison of the proposed antenna among other literature is concluded. This work has the advantages of simple design, high gain, low cost, and broadband operation, which have potential applications in satellite communication.

Reference	Central Frequency	Antenna Polarization	Feed Polarization	Unit Polarization	Feed Type	Impedance Bandwidth	3-dB AR Bandwidth
[18]	26.0 GHz	CP	CP	CP	SIW antenna	31.0%	20.0%
[25]	40 GHz	CP	CP	CP	Horn	--	>25.0%
[27]	26.5 GHz	CP	LP	LP to CP	SIW antenna	1.5%	13.6%
[28]	10 GHz	CP	LP	LP to CP	Horn	--	25.1%
[29]	13 GHz	CP	LP	LP to CP	Microstrip patch	12.4%	16.6%
This work	**9.5 GHz**	**CP**	**LP**	**LP**	**Microstrip patch**	**20.1%**	**21.0%**

Tab. 1. Performance comparison of the proposed antenna among other literature.

Acknowledgments

This work was supported by the National Natural Science Foundation of China (No. 62171460, 62371466), the Natural Science Basic Research Program of Shaanxi Province, China (No. 2022JM-319, 2022JQ-685, 20220104, 20210110 and 2020022) and the Postdoctoral Innovative Talents Support Program of China (No. BX20180375, 2019M653960).

References

[1] ZHU, X. W., GAO, J., CAO, X. Y., et al. A novel low-RCS and wideband circularly polarized patch array based on metasurfece. *Radioengineering*, 2019, vol. 29, no. 1, p. 99–107. DOI: 10.13164/re.2019.0099

[2] YANG, B., YU, Z., LAN, J., et al. Digital beamforming-based massive MIMO transceiver for 5G millimeter-wave communications. *IEEE Transactions on Microwave Theory and Techniques*, 2018, vol. 66, no. 7, p. 3403–3418. DOI: 10.1109/TMTT.2018.2829702

[3] ZHANG, Z., ZHAO, Y., JI, L., et al. Design of multi-beam antenna based on Rotman lens. *International Journal of RF and Microwave Computer-Aided Engineering*, 2018, vol. 28, no. 2, p. 1–10. DOI: 10.1002/mmce.21192

[4] CHENG, Y. J., CHEN, P., HONG, W., et al. Substrate-integrated-waveguide beamforming networks and multibeam antenna arrays for low-cost satellite and mobile systems. *IEEE Antennas & Propagation Magazine*, 2011, vol. 53, no. 6, p. 18–30. DOI: 10.1109/MAP.2011.6157710

[5] TENGAH, Z., ABD RAHMAN, N. H., YAMADA, Y. Design of bifurcated beam using convex bent array feed for satellite mobile earth station application. *Radioengineering*, 2022, vol. 31, no. 4, p. 541–552. DOI: 10.13164/re.2022.0541

[6] CAMERON, T. R., ELEFTHERIADES, G. V. Analysis and characterization of a wide-angle impedance matching metasurface for dipole phased arrays. *IEEE Transactions on Antennas and Propagation*, 2015, vol. 63, no. 9, p. 3928–3938. DOI: 10.1109/TAP.2015.2448231

[7] BENINI, A., MARTINI, E., MONNI, S., et al. Phase-gradient meta-dome for increasing grating-lobe-free scan range in phased arrays. *IEEE Transactions on Antennas and Propagation*, 2018, vol. 66, no. 8, p. 3973–3982. DOI: 10.1109/TAP.2018.2835575

[8] GANDINI, E., SILVESTRI, F., BENINI, A., et al. A dielectric dome antenna with reduced profile and wide scanning capability. *IEEE Transactions on Antennas and Propagation*, 2021, vol. 69, no. 2, p. 747–759. DOI: 10.1109/TAP.2020.3022960

[9] MONTI, A., VELLUCCI, S., BARBUTO, M., et al. Quadratic-gradient metasurface-dome for wide-angle beam-steering phased array with reduced gain loss at broadside. *IEEE Transactions on Antennas and Propagation*, 2023, vol. 71, no. 2, p. 2022–2027. DOI: 10.1109/TAP.2022.3222716

[10] CHENG, X., YAO, Y., TOMURA, T., et al. A compact multi-beam end-fire circularly polarized septum antenna array for millimeter-wave applications. *IEEE Access*, 2018, vol. 6, p. 62784 to 62792. DOI: 10.1109/ACCESS.2018.2876872

[11] KUMAR, S., VISHWAKARMA, R. K., KUMAR, R., et al. Slotted circularly polarized microstrip antenna for RFID application. *Radioengineering*, 2017, vol. 26, no. 4, p. 1025–1032. DOI: 10.13164/re.2017.1025

[12] CAO, Y., YAN, S., LI, J., et al. A pillbox based dual circularly-polarized millimeter-wave multi-beam antenna for future vehicular radar applications. *IEEE Transactions on Vehicular Technology*, 2022, vol. 71, no. 7, p. 7095–7103. DOI: 10.1109/TVT.2022.3162299

[13] NADI, M., RAJABALIPANAH, H., CHELDAVI, A., et al. Flexible manipulation of emitting beams using single-aperture circularly polarized digital metasurface antennas: Multi-beam radiation toward vortex beam generation. *Advanced Theory and Simulations*, 2020, vol. 3, no. 4, p. 1–11. DOI: 10.1002/adts.201900225

[14] LI, S. J., LI, Z. Y., HAN, B. W., et al. Multifunctional coding metasurface with left and right circularly polarized and multiple beams. *Frontiers in Materials*, 2022, vol. 9, p. 1–9. DOI: 10.3389/fmats.2022.854062

[15] JEONG, M. G., KIM, J. H., BAE, S. H., et al. Miniaturised multi-beam-controlled circular eight-port beamforming network for long-range UHF RFID hemispheric coverage. *IET Microwaves Antennas & Propagation*, 2018, vol. 12, no. 2, p. 154–159. DOI: 10.1049/iet-map.2017.0416

[16] JOO, T., KIM, Y., HWANG, C., et al. Design of multi-beam active phased array antenna system for aerial communications (in Korean). *Journal of Korean Institute of Electromagnetic Engineering and Science*, 2021, vol. 32, no. 4, p. 334–343. DOI: 10.5515/KJKIEES.2021.32.4.334

[17] AL-SADOON, M., PATWARY, M., ZAHEDI, Y., et al. A new beamforming approach using 60 GHz antenna arrays for multi-beams 5G applications. *Electronics*, 2022, vol. 11, no. 11, p. 1–22. DOI: 10.3390/electronics11111739

[18] JIANG, Z. H., ZHANG, Y., XU, J., et al. Integrated broadband circularly polarized multibeam antennas using berry-phase transmit-arrays for Ka-band applications. *IEEE Transactions on Antennas and Propagation*, 2020, vol. 68, no. 2, p. 859–872. DOI: 10.1109/TAP.2019.2944547

[19] DUDEK, A., KANIOS, P., STASZEK, K., et al. Octave-band four-beam antenna arrays with stable beam direction fed by broadband 4×4 Butler matrix. *Electronics*, 2021, vol. 10, no. 21, p. 1–14. DOI: 10.3390/electronics10212712

[20] ANSARI, A. E., DAS, S., TABAKH, I., et al. Design and realization of a broadband multi-beam 1×2 array antenna based on 2×2 Butler matrix for 2.45 GHz RFID reader applications. *Journal of Circuits, Systems and Computers*, 2022, vol. 31, no. 17, p. 1–20. DOI: 10.1142/S0218126622503054

[21] CHEN, P., HONG, W., KUAI, Z., et al. A double layer substrate integrated waveguide Blass matrix for beamforming applications. *IEEE Microwave and Wireless Components Letters,* 2009, vol. 19, no. 6, p. 374–376. DOI: 10.1109/lmwc.2009.2020020

[22] VANI, T. D., SUBHASHINI, K. R. Design approach of multibeam using phased array antenna aided with Butler matrix for a fixed coverage area. *Progress in Electromagnetics Research B*, 2018, vol. 80, p. 133–149. DOI: 10.2528/PIERB18011012

[23] LIMA, E. B., MATOS, S. A., COSTA, J. R., et al. Circular polarization wide-angle beam steering at Ka-band by in-plane translation of a plate lens antenna. *IEEE Transactions on Antennas and Propagation*, 2015, vol. 63, no. 12, p. 5443–5455. DOI: 10.1109/TAP.2015.2484419

[24] LEE, C. H., HOANG, T. V., CHI, S. W., et al. Low-profile quad-beam circularly polarised antenna using transmissive metasurface. *IET Microwaves, Antennas and Propagation*, 2019, vol. 13, no. 10, p. 1690–1698. DOI: 10.1049/iet-map.2018.6056

[25] JIANG, Z. H., KANG, L., YUE, T., et al. Wideband transmit arrays based on anisotropic impedance surfaces for circularly polarized single-feed multibeam generation in the Q-band. *IEEE*

Transactions on Antennas and Propagation, 2020, vol. 68, no. 1, p. 217–229. DOI: 10.1109/TAP.2019.2943343

[26] YANG, Y., BAN, Y. L., YANG, Q., et al. Millimeter wave wide-angle scanning circularly polarized antenna array with a novel polarizer. *IEEE Transactions on Antennas and Propagation*, 2022, vol. 70, no. 2, p. 1077–1086. DOI: 10.1109/TAP.2021.3111255

[27] YU, Z. Y., ZHANG, Y. H., HE, S. Y., et al. A wide-angle coverage and low scan loss beam steering circularly polarized folded reflectarray antenna for millimeter-wave applications. *IEEE Transactions on Antennas and Propagation*, 2022, vol. 70, no. 4, p. 2656–2667. DOI: 10.1109/TAP.2021.3118790

[28] ZHANG, P. P., ZHU, X. C., HU, Y., et al. A wideband circularly polarized folded reflectarray antenna with linearly polarized feed. *IEEE Antennas and Wireless Propagation Letters*, 2022, vol. 21, no. 5, p. 913–917. DOI: 10.1109/LAWP.2022.3151622

[29] CHEN, J. H., LI, G. W., GE, Y. H., et al. Broadband circularly polarized multi-beam folded transmitarray antenna. *International Journal of RF and Microwave Computer-Aided Engineering*, 2022, vol. 32, no. 7, p. 1–9. DOI: 10.1002/mmce.23161

[30] WANG, H., DONG, X. F., SHEN, J., et al. Fan-beam antenna design based on metasurface lenses. *International Journal of RF and Microwave Computer-Aided Engineering*, 2021, vol. 31, no. 4, p. 1–8. DOI: 10.1002/mmce.22582

[31] HALL, P. S. Application of sequential feeding to wide bandwidth, circularly polarised microstrip patch arrays. *IEE Proceedings H (Microwaves, Antennas and Propagation)*, 1989, vol. 136, no. 5, p. 390–398. DOI: 10.1049/ip-h-2.1989.0070

[32] HALL, P. S., SMITH, M. S. Sequentially rotated arrays with reduced sidelobe levels. *IEE Proceedings - Microwaves, Antennas and Propagation*, 1994, vol. 141, no. 4, p. 321–325. DOI: 10.1049/ip-map_19941193

[33] SMOLDERS, A. B., VISSER, H. J. Low side-lobe circularly-polarized phased arrays using a random sequential rotation technique. *IEEE Transactions on Antennas and Propagation*, 2014, vol. 62, no. 12, p. 6476–6481. DOI: 10.1109/TAP.2014.2359476

About the Authors ...

Zexu GUO received a B.S. degree from Beijing Jiaotong University (BJTU) in 2018. He is the 2018 Beijing Excellent Graduate. He received an M.S. degree from the Air Force Engineering University (AFEU) in 2020. He is currently working towards his Ph.D. degree in AFEU. In his research, he specializes in metasurface, transmitarray, polarization converter design, and RCS reduction techniques.

Yulong ZHOU (corresponding author) received the B.S. and M.S. degrees from the Air Force Engineering University, China, in 2015 and 2017, respectively, and the Ph.D. degree from the National University of Singapore, Singapore, in 2022. Since 2023, he has been with the Air Force Engineering University, China, where he is currently a Lecturer. Dr. Zhou was a recipient of the Best Student Paper Competition Award at ACES-China 2021 and 2022 Best Student Paper Competition Award in the IEEE Singapore MTT/AP Joint Chapter. His research interests include metasurface design, electromagnetic inverse scattering, and its application in non-destructive imaging.

Huanhuan YANG received the M.S. and Ph.D. degrees from the Air Force Engineering University (AFEU), Xi'an, China, in 2012 and 2016, respectively. He was a joint-supervision Ph.D. student of AFEU and Tsinghua University. He is currently an Associate Professor at AFEU. His research interests include advanced antenna array, reconfigurable antenna, reflectarray, metasurface, and RCS reduction technique.

Sijia LI received a B.S. degree from Guangxi University, Nanning, China, in 2009. He received his M.S. and Ph.D. degrees from the Air Force Engineering University in 2011 and 2015, respectively. He joined the Air Force Engineering University as a Lecturer in 2015 and became an Associate Professor in 2017. Since 2019, he has been engaged in postdoctoral research at the Southeast University. His research activity has been focused on the multifunctional metasurface and its application for RCS reduction of antennas.

Tong LI received her B.S. and Ph.D. degrees in Electronic and Information Engineering from Xidian University, Xi'an, China, in 2010 and 2015, respectively. She is currently an Associate Professor at AFEU. Her research interests include ultra-wideband communication devices, RCS reduction techniques, reconfigurable antennas, and metasurface.

Xiangyu CAO received the B.S. and M.S. degrees from the Air Force Missile Institute (AFEI), Xi'an, China, in 1986 and 1989, respectively, and the Ph.D. degree in AFEU, Xi'an, China, in 1999, all in Electrical Engineering. She joined AFEI in 1989 as an Assistant Teacher and became an Associate Professor in 1996. From 1999 to 2002, she was engaged in postdoctoral research at Xidian University, China. She was a Senior Research Associate at the City University of Hong Kong from 2002 to 2003.